Available online at www.sciencedirect.com
SCIENCE DIRECT®
Computational Materials Science 34 (2005) 173–187
COMPUTATIONAL MATERIALS SCIENCE
www.elsevier.com/locate/commatsci

Large-scale modeling of carbon-nanotube composites by a fast multipole boundary element method

Yijun Liu [a,*], Naoshi Nishimura [b], Yoshihiro Otani [b]

[a] *Department of Mechanical, Industrial and Nuclear Engineering, University of Cincinnati, P.O. Box 210072, Cincinnati, OH 45221-0072, USA*
[b] *Academic Center for Computing and Media Studies, Kyoto University, Kyoto 606-8501, Japan*

Received 4 October 2004; accepted 30 November 2004

Abstract

Carbon nanotubes (CNTs) exhibit extremely high stiffness and strength, and are regarded as perfect reinforcing fibers for developing a new class of nanocomposites. The use of atomistic or molecular dynamics (MD) simulations is inevitable for the analysis of such nanomaterials in order to study the *local* load transfers, interface properties, or failure modes at the nanoscale. Meanwhile, continuum models based on micromechanics have been shown in several recent studies to be useful in the *global* analysis for characterizing such nanomaterials at the micro- or macro-scale. In this paper, a new continuum model of the CNT-based composites is developed for large-scale analysis at the micro-scale in order to characterize such composites. In this new approach, CNTs are treated as rigid fibers in the elastic matrix, due to its high stiffness that are at least two orders higher than those of most polymer matrices. A recently developed fast multipole boundary element method (BEM) is employed to solve the boundary integral equations governing this rigid-inclusion problem. Numerical examples of CNT composites, with the number of CNT fibers considered reaching 16,000 and total degrees of freedom above 28.8 millions, are solved successfully by the fast multipole BEM. Effective elastic moduli of the CNT-composite models are evaluated and compared favorably with other reported data based on an MD and multiscale approach. The developed BEM is demonstrated to be a very promising first-order tool for large-scale modeling and characterizations of CNT-based composites.

Keywords: Carbon-nanotube composites; Rigid inclusions; Fast boundary element method

1. Introduction

Carbon nanotubes possess extremely high stiffness, strength and resilience, and are

* Corresponding author. Tel.: +1 513 556 4607; fax: +1 513 556 3390.
E-mail address: yijun.liu@uc.edu (Y.J. Liu).

0927-0256/$ - see front matter © 2005 Elsevier B.V. All rights reserved.
doi:10.1016/j.commatsci.2004.11.003

considered by many to be the ideal reinforcing fibers for an entirely new class of composite materials [1–5]. There has been tremendous interest in the modeling and simulations of the CNT composites in order to characterize their mechanical properties for potential engineering applications. Both molecular dynamics, continuum mechanics, and combinations of both, have been attempted for this purpose. MD approach is necessary in the study of nanocomposites, especially for investigations of the local interactions of CNTs with matrix materials, interface properties, or failure modes. However, MD simulations at present are limited to small length and time scales, due to the limitations of the current computing power. For example, all current MD simulation results of CNT composites have been limited to models with only a single CNT in a matrix. CNT fibers in a real composite are likely to have different shapes and sizes. They can be straight or curved, short or long, aligned or oriented arbitrarily, and distributed randomly. All these factors make the estimates of the mechanical properties of CNT composites very difficult using only the MD approach, if not impossible. Large-scale representative volume elements (RVEs) with hundreds or thousands of CNT fibers may deemed necessary in characterizing CNT composites. Continuum mechanics approaches can fill this gap and results from such approaches have been shown to be surprisingly close to those of the MD-based simulations in modeling CNT composites.

Continuum mechanics approaches have been applied successfully for simulations of the mechanical responses of individual CNTs which are treated as beams, thin shells or solids in cylindrical shapes [6–11]. Although efficient in computing and able to handle models at larger length scales, simulation results obtained using the continuum mechanics approaches should be interpreted correctly. Attentions should be paid to the overall deformations or load transfer mechanisms, rather than to local properties, such as those at the interface between CNTs and a matrix, where the physics should be addressed by MD simulations. Characterization of a CNT composite requires only the knowledge of its global responses, such as the displacement and stress fields at the boundaries of an RVE. Thus the continuum mechanics approaches may be adequate and sufficient in modeling CNT composites in this regard. Some research results along this line have demonstrated the usefulness of the continuum approaches.

Pipes and Hubert's work [12] seems to be the first among others in characterizing CNT composites using a continuum mechanics approach. Applying the traditional textile-mechanics approach and anisotropic elasticity theory, they studied the behavior of a CNT composite wherein the fibers are layered cylinders with layers containing arrays of CNTs arranged to form a hexagonal cross-section and following a helical curve. Stress distributions and effective elastic properties are evaluated in [12] using the two continuum mechanics approaches. Liu and Chen [13–15] applied the finite element and boundary element methods (FEM/BEM) for the study of CNT composite models, where RVEs containing one or multiple CNTs are modeled as thin elastic layer in the shape of a capsule (for short CNT) or an open cylinder (for long CNT). Effective elastic properties of the CNT composites are evaluated and compared with the rules of mixtures (including an extended rule of mixture derived for short-fiber composites). The detailed FEM models in [14,15] reveal that the "stress" gradient cross the interface of the CNT and matrix is very high and the number of elements can become prohibitively large for the FEM in large-scale modeling of CNT composites, if the continuum models can be used. Fisher et al. [16,17] employed the FEM to study the effect of the waviness of CNT fibers in a CNT composite. Their FEM model predicts that even slight curvature of the CNTs can result in significant decrease of the effective stiffness of the CNT composites, which is consistent with experimental observations. Due to the large size of the FEM model for detailed 3-D studies, the RVE used in [16,17] contains only a segment of a CNT with the surrounding matrix material. All the above mentioned investigations based on the continuum approaches suggest that micromechanics is still relevant and useful in the study of CNT composites for characterizations based on the global responses of CNT composites. The results of MD-based

multiscale and full MD approaches for characterizing CNT composites also support this claim.

Odegard, Gates, and others published the most comprehensive results in Ref. [18] on evaluations of effective elastic properties of CNT composites using an MD-based multiscale approach. They combined the MD simulation with the micromechanics approach using the equivalent-continuum model they developed earlier [19]. In their approach, the MD is employed to calculate the properties of an effective fiber that contains a CNT surrounded by the polymer in a cylindrical shape. This effective fiber is then used in the micromechanics homogenization model for evaluations of the effective properties of the CNT composites. Results of computed effective Young's moduli and shear moduli using this approach are presented for different CNT lengths and volume fractions. Direct comparison of the computed results with the available experimental data is also provided and good agreement is shown in Ref. [18]. Interestingly, this multiscale approach is also compared with the continuum approach developed by Pipes and Hubert in Ref. [12] in a recent paper [20]. Overlap of the results of the two different models is shown for a large range of CNT volume fractions for a CNT-polymer composite with the CNT fiber length equal to 500 nm. It is also stated in Ref. [20] that results obtained by the two methods are in general about 15% lower than those predicted by the classical rule of mixtures. This paper, Ref. [20], seems to be a direct validation of the micromechanics approach for characterizing the CNT composites.

Most recently, Griebel and Hamaekers [21] carried out a detailed study on evaluating the effective properties of CNT-polymer composites using the molecular dynamics approach. Two MD models of the CNT composites were considered, one with a short single-walled carbon nanotube (of 6 nm in length) in the polymer, and the other with an infinitely long one. To reduce the computational complexity, a united-atom potential is also proposed for modeling the polymer, besides the full Brenner potential [21]. Their MD models predict that along the CNT direction, the effective elastic modulus is about two times of the polymer modulus for the short CNT case (with a CNT volume fraction of 2.8%), and about thirty times higher for the long CNT case (with a CNT volume fraction of 6.5%). They also compared their MD results with those using the rules of mixtures. Surprisingly, the MD predictions are found to be within the range of those by using the rules of mixtures, with the largest decrease being 15% for the long CNT case and the largest increase being 25% for the short CNT case, compared with the results using the rules of mixtures [21]. The MD models and rules of mixtures are two drastically different models in the two theories covering two different length scales and their close correlations need further attention. All the above mentioned results from MD and MD-based equivalent continuum approaches again suggest that the continuum approaches may be within the range of accuracy for engineering applications in characterizing CNT composites at the micro- or macro-scales.

If the continuum approaches are adequate for characterizing the CNT composites, a natural question will be: what is the most appropriate continuum model for large-scale modeling of such composites that can capture the overall mechanical behaviors while without exhausting the current computing resources? Based on the extremely high stiffness of the CNTs, one simple choice will be to treat them as rigid slender inclusions in a relatively soft matrix material, such as polymers which are the main matrix materials now for developing CNT composites. Study of the feasibilities of this seemingly naïve rigid-fiber approach in modeling CNT composites is the main subject of this paper.

In this paper, a new continuum model of the CNT-based composites is developed for large-scale analysis at the micro-scale in order to characterize such nanocomposites. In this new approach, CNTs are treated as rigid fibers in the elastic matrix, due to its high stiffness that are at least two orders higher than those of most polymer matrices. A recently developed fast multipole boundary element method is employed to solve the boundary integral equations governing this rigid-inclusion problem. Numerical examples of CNT composites, with the number of CNTs considered reaching 16,000 and total degrees of freedom above 28.8 millions, are successfully solved by the fast multipole BEM. Effective elastic moduli of the

CNT-composite models are evaluated and compared with other reported data based on a multiscale approach. Good agreement of the results from the fast multipole BEM and the multiscale approach is observed. The developed fast multipole BEM is demonstrated to be a very promising tool for large-scale analysis of CNT-based composites for their characterizations.

The rest of this paper is organized as follows: In Section 2, the justification of why CNTs might be treated as rigid inclusions in an elastic matrix material is attempted and related papers in the literature are reviewed. In Section 3, the boundary integral equation (BIE) governing the elastic fields of an elastic domain embedded with rigid inclusions is presented. The fast multipole BEM used to solve the BIE is also introduced in Section 3. Numerical examples of modeling CNT composites are presented in Section 4. Advantages, limitations and potential applications of the developed fast multipole BEM approach are offered in Section 5. The paper concludes with Section 6.

2. The rigid-inclusion model of CNT composites

Carbon nanotubes, either single-walled or multi-walled, have been found to have very large elastic moduli along their axis direction, with an averaged value around 1 TPa, as reported in the literature [2,3,6,22–25]. This high elastic modulus is at least two orders of magnitude higher than those of most polymers whose elastic moduli are around 4 GPa. Therefore, it is safe to assume the stiffness of the CNT is infinitely large relative to that of the polymer matrix when studying the CNT-polymer composite properties, from the mathematical point of view. Even for other matrix materials with larger Young's moduli, this can also be a first approximation. Limited experimental results and MD simulations also revealed this phenomenon and suggested this assumption. Fig. 1 shows a recent MD simulation of a CNT fiber pullout from a polymer. Picture on the left is the initial configuration of the CNT with surrounding polymer molecules. Picture on the right is a snapshot after the pullout of the CNT from the polymer. The fiber is a (10, 10) single-walled CNT with a diameter of 13.56 Å and a length of about 53 Å. Details on the applied potentials, boundary conditions, time step, numerical integration scheme, and others can be found in Ref. [26]. It is observed from Fig. 1 that the CNT experiences little or no deformation at all during the pullout simulation and behaves like a rigid "rod", while the polymer deforms significantly in the process (a recent study in Ref. [27] also shows a similar phenomenon). It is true that CNTs are very flexible in the lateral direction when they are under bending. Will the rigid-inclusion model still be valid? The answer is "yes", if structures made of CNT composites are under consideration. Even

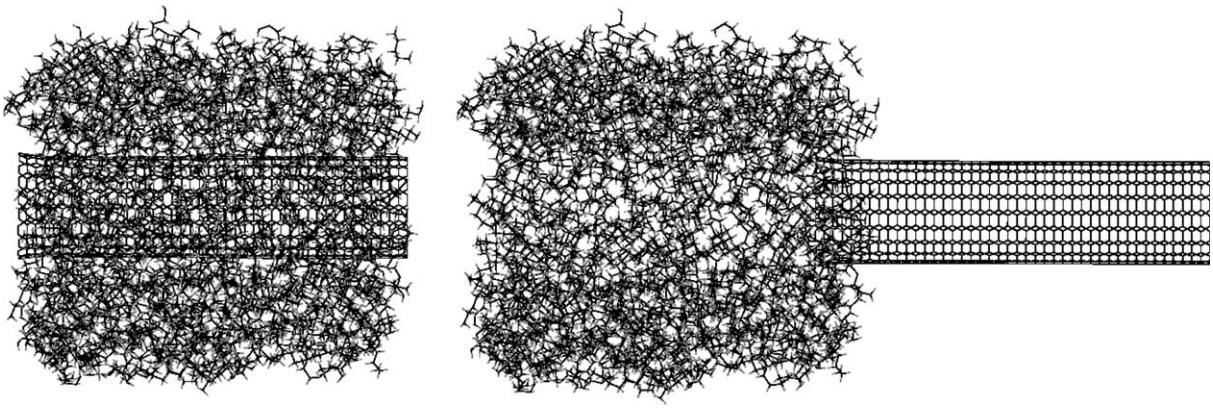

Fig. 1. An MD simulation of the pullout of a CNT from a polymer matrix, which reveals little deformation of the CNT relative to the polymer matrix (see Ref. [26] for more details).

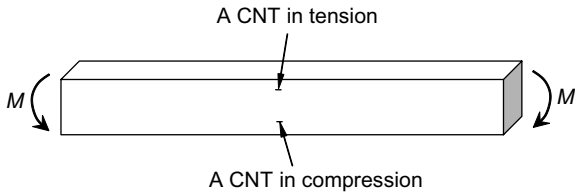

Fig. 2. A structural block made of CNT composite under a bending load M: the relatively small and straight CNTs are likely either in tension or compression along their axial directions.

when a structure at the micro- or macro-scales sustains bending loads, each CNT, like a fiber or tiny material point in the structure, is likely to be in tension or compression only. This is illustrated in Fig. 2. However, if the CNTs are curved, cautions should be used in the rigid-inclusion model and further studies are needed. This paper will address straight CNT fibers only at present, which is also the target of the CNT-composite development due to the maximum enhancement that straight CNT fibers can deliver.

Rigid-inclusion problems have been studied for some time in applied mechanics using the integral equation approaches [28]. In the case of stress analysis of rigid-line inclusions, also called anti-cracks in a 2-D elastic domain [29], many research results have been reported in the literature. Hu et al. [30–34] carried out extensive studies of rigid-line inclusions in a matrix using the integral equation methods for 2-D cases. The interactions of rigid lines with cracks and the effects of rigid lines on the effective elastic material properties of composites were successfully studied using this approach for 2-D models [30–34]. Recently, Leite et al. [35] reported a 2-D BEM coupled with finite elements that are used to model the bar inclusions in a matrix. The displacement and stress fields near the line inclusions are studied by this approach. In another recent work [36], Dong et al. developed a hypersingular BIE approach for the analysis of interactions of rigid-line inclusions with cracks in a 2-D elastic medium. Stress intensity factors at the tips of rigid lines are computed and compared with analytical solutions. In all the results mentioned above, only 2-D models with a few (less than 10) rigid-line inclusions were considered.

In the context of modeling fiber-reinforced composites using 3-D rigid-inclusion models, Ingber and Papathanasiou's work [37,38] seems to be the first reported one using the BEM. The full conventional BIE for Navier's equation governing an *incompressible* medium containing rigid fibers is solved in [37,38] in order to determine the effective moduli of composites with different fiber volume fractions and aspect ratios. Constant boundary elements were employed to discretize the BIE which contains the singular as well as weakly-singular kernels. Up to 200 short, aligned rigid fibers, with the total degrees of freedom (DOFs) of about 12,000, were successfully solved by the developed BEM approach in [38]. Very good agreement of the evaluated effective moduli using their BEM approach and analytical results is reported in [38], which demonstrates that the rigid-fiber model is very promising and the BEM is very efficient for characterizations of fiber-reinforced composites.

3. The BEM for rigid-inclusion problems

Consider a 3-D infinite elastic domain V embedded with n rigid inclusions (Fig. 3). Perfect bonding conditions are assumed between the rigid inclusions and elastic matrix. The matrix is loaded with a remote stress or displacement field. The displacement at a point inside the domain V is given

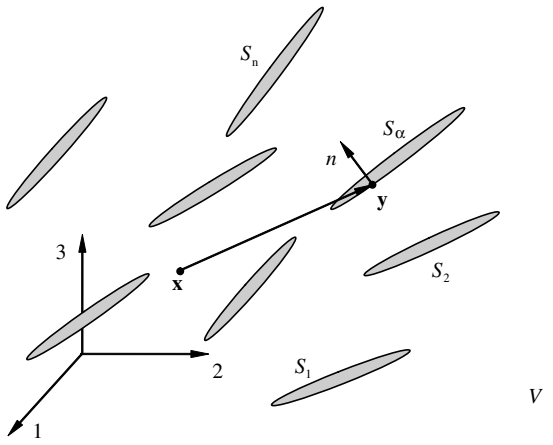

Fig. 3. A 3-D infinite elastic medium V embedded with rigid fibers.

by the following representation integral (see, e.g., [39–41]):

$$\mathbf{u}(\mathbf{x}) = \int_S [\mathbf{U}(\mathbf{x},\mathbf{y})\mathbf{t}(\mathbf{y}) - \mathbf{T}(\mathbf{x},\mathbf{y})\mathbf{u}(\mathbf{y})]\mathrm{d}S(\mathbf{y}) + \mathbf{u}^{\infty}(\mathbf{x}), \quad \forall \mathbf{x} \in V, \tag{1}$$

where $\mathbf{u}$ and $\mathbf{t}$ are the displacement and traction vectors, respectively; $S = \cup_\alpha S_\alpha$ with S_α being the boundary of the α-th rigid inclusion (Fig. 3); and $\mathbf{u}^{\infty}$ the undisturbed displacement field due to the remote stress or displacement field. For a finite (interior) domain, this term will not present in Eq. (1). The two kernel functions $\mathbf{U}(\mathbf{x},\mathbf{y})$ and $\mathbf{T}(\mathbf{x},\mathbf{y})$ in Eq. (1) are the displacement and traction components of the fundamental solution (Kelvin's solution), respectively, which can be found in any references on the BEM (see, e.g., [39–41]).

For a rigid inclusion enclosed by S_α, the displacement at any point $\mathbf{y}$ can be described by the rigid-body motions as:

$$\mathbf{u}(\mathbf{y}) = \mathbf{d} + \boldsymbol{\omega} \times \mathbf{p}(\mathbf{y}), \tag{2}$$

where $\mathbf{d}$ is the rigid-body translational displacement vector, $\boldsymbol{\omega}$ the rotation vector and $\mathbf{p}$ a position vector for point $\mathbf{y}$ measured from a reference point (such as the center of the inclusion). Considering the BIE for the rigid inclusion itself in the domain enclosed by S_α and equilibrium of the tractions at the interface, and assuming perfect bonding between the inclusions and matrix, it can be shown that the second integral in Eq. (1) containing the traction kernel vanishes for rigid inclusions [42]. Therefore, Eq. (1) reduces to:

$$\mathbf{u}(\mathbf{x}) = \int_S \mathbf{U}(\mathbf{x},\mathbf{y})\mathbf{t}(\mathbf{y})\mathrm{d}S(\mathbf{y}) + \mathbf{u}^{\infty}(\mathbf{x}), \quad \forall \mathbf{x} \in V, \tag{3}$$

for all *rigid* inclusions ($S = \cup_\alpha S_\alpha$). This integral is applied to evaluate the displacement field at any point inside the domain V, once the tractions on the surfaces of the rigid inclusions are obtained. The stress field at any point in the domain can also be evaluated by taking derivatives of expression (3) and applying the Hook's law (see, e.g., [39–41]).

By letting the source point $\mathbf{x}$ approach the boundary S in Eq. (3), one arrives at the following boundary integral equation:

$$\mathbf{u}(\mathbf{x}) = \int_S \mathbf{U}(\mathbf{x},\mathbf{y})\mathbf{t}(\mathbf{y})\mathrm{d}S(\mathbf{y}) + \mathbf{u}^{\infty}(\mathbf{x}), \quad \forall \mathbf{x} \in S = \cup_\alpha S_\alpha, \tag{4}$$

which is used to solve for the unknown tractions at the interfaces between the inclusion and matrix. This BIE for rigid-inclusion problems is extremely compact and simple, in which only the weakly-singular kernel needs to be handled. More details in deriving this equation can be found in a recent related work [42].

There are additional unknowns in Eq. (4), that is, the rigid-body motions of each inclusion, expressed by Eq. (2) that contains six unknowns ($\mathbf{d}$ and $\boldsymbol{\omega}$ vectors) for each inclusion. Additional equations are needed to supplement BIE (4). These equations can be obtained by considering equilibrium of each inclusion, that is, the following six scalar equations:

$$\int_{S_\alpha} \mathbf{t}(\mathbf{y})\mathrm{d}S(\mathbf{y}) = \mathbf{0}; \tag{5}$$

$$\int_{S_\alpha} \mathbf{p}(\mathbf{y}) \times \mathbf{t}(\mathbf{y})\mathrm{d}S(\mathbf{y}) = \mathbf{0}; \tag{6}$$

for $\alpha = 1, 2, \ldots, n$. Eq. (5) represents the equilibrium of the forces, while expression (6) that of the moments, for each rigid inclusion. BIE (4) and Eqs. (2), (5) and (6) are simultaneously solved to obtain the unknown rigid-body motions $\mathbf{d}$ and $\boldsymbol{\omega}$, and traction $\mathbf{t}$ for all the inclusions.

The boundary element method is employed to discretize and solve the system of equations (2) and (4)–(6) in this study. The BEM is a natural way to solve the BIE, due to its reduction of the dimension of the problem domain and high accuracy. With the development of the fast multipole methods (FMM) (see a recent review in Ref. [43]) for solving boundary integral equations, large models with several million degrees of freedom can be solved readily on a desktop computer. The main idea of the fast multipole methods is that elements of integration are grouped into clusters (cells) according to the distance of the elements to the source point. The integrations on elements in one cluster are computed together using multipole expansions. Thus, the number of integrations is reduced and hence the computing time. In addi-

tion, with the use of iterative solvers (such as GMRES), the full BEM matrix is never formed explicitly in the fast multipole methods and thus the required memory is also much less for the multipole BEM. Using the FMM for the BEM, the solution time of a problem is reduced to order $O(N)$, instead of $O(N^2)$ as in the traditional BEM (with N here being the number of equations). In recent years, the FMM has also been demonstrated to be especially good for solving problems with large numbers of cracks and inclusions in both 2-D and 3-D cases. Some of the work on solving inclusion problems using the FMM BIE/BEM can be found in Refs. [44–48]. The details of the FMM BEM formulation and implementation used in this study, including the choice of preconditioners and other parameters used in the FMM, can be found in Refs. [42,43,49,50].

4. Numerical examples

The representative volume elements used in this study are discussed first. Then the fast multipole BEM developed is used to study an example of short-fiber composites and the results are compared with the theoretical prediction for verifications. Results in modeling CNT composites using the developed fast multipole BEM based on the rigid-inclusion model are presented in the last subsection. These BEM results are compared against those using the MD-based multiscale equivalent-continuum approach reported in Ref. [18], because the latter have been verified with the experimental data [18] and also shown to be consistent with those by using other continuum mechanics based models in Ref. [20].

4.1. The representative volume elements (RVEs) used

The representative volume elements considered in this work are embedded in the infinite domain filled with the same material as that of the matrix (Fig. 4). The CNT fibers are dispersed within the RVEs which are of finite sizes. In this way, an exterior problem can be solved using the fast multipole BEM, where boundary elements are only needed at the interfaces of the fibers and the matrix. Although the fast multipole BEM can also solve

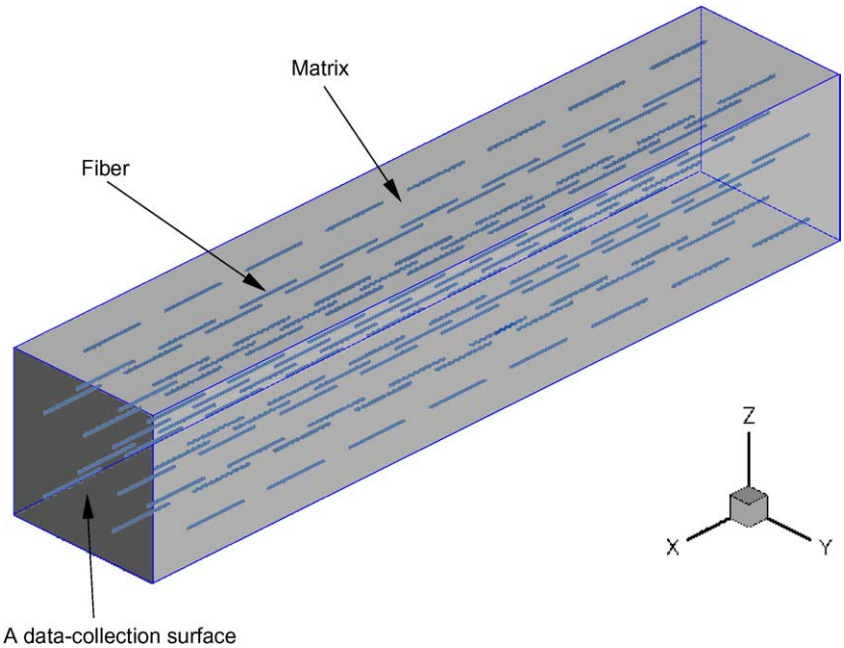

Fig. 4. A representative volume element for studying fiber-reinforced composites.

interior-type of problems, it converges much slower than in the case of an exterior problem. Thus, we choose to study the exterior problem first. Data-collection surfaces will either coincide with the surfaces of the RVE or be inside the RVEs (Fig. 4). The displacement and stresses will be calculated on these data-collection surfaces. Then, the values of these displacements and stresses will be employed to evaluate the effective properties of the composites.

A far-field uniaxial tensile stress σ^{∞} is applied to the infinite domain V only in the fiber direction (the x-direction, Fig. 4). The effective modulus of the composite in the fiber direction is estimated using the displacement and stress results at two data-collection surfaces normal to the x-axis by the following formula:

$$E_{\text{eff}} = \frac{(\sigma_x)_{(\text{ave})} L}{(\Delta u_x)_{(\text{ave})}}, \tag{7}$$

where E_{eff} is the estimated effective modulus of the composite in the x-direction, $(\Delta u_x)_{(\text{ave})}$ and $(\sigma_x)_{(\text{ave})}$ are the averaged elongation and stress of the RVE, respectively, evaluated at the two data-collection surfaces normal to the x-directions (Fig. 4), and L is the distance between the two data-collection surfaces. More discussions on the RVEs used in this work can be found in Ref. [42].

Triangular constant boundary elements are employed in the discretization of the interfaces between the fibers and the matrix. Three corner nodes are used to define the geometry of a triangular element. However, the field over the element is only represented by its value at the center for each element. Thus, each element will have three degrees of freedom (unknown traction components in this case) for constant elements. All the integrals are integrated analytically so that accurate results are ensured even when fibers are packed tightly and surfaces are very close to each other.

4.2. Study of short-fiber composites

To verify the developed BEM approach for analyzing fiber-reinforced composites, we first study the models of short-fiber reinforced composites, for which theoretical predictions, using, e.g., the Halpin–Tsai equation, are available. This is the same approach adopted in Ingber and Papathanasiou's work [37,38]. In the limit as the ratio of the fiber stiffness to matrix stiffness tends to infinity (thus a rigid-fiber case), the Halpin–Tsai equation can be written as (see, e.g., Refs. [37,38]):

$$\frac{E_{\text{composite}}}{E_{\text{matrix}}} = \frac{1 + 2\xi\phi}{1 - \phi}, \tag{8}$$

where $E_{\text{composite}}$ and E_{matrix} are the longitudinal modulus of the composite and matrix, respectively; $\xi = l/2r$ is fiber aspect ratio (with l being the length and r the radius of the fiber); and ϕ is the volume fraction of the fibers in the composite. Eq. (8) will be used to verify the BEM estimates of the effective longitudinal modulus.

An array of $10 \times m \times m$ short fibers (capsule-like) with $l = 8$ and $r = 1$ are placed in a cubical RVE of a fixed dimension $100 \times 100 \times 100$. The cases studied include $m = 5$, 10, 14, 18, 22, 24, 26, 28, 30, 32, 34, and 36, for which the corresponding volume fractions of the fibers change from 0.58%, 2.30%, ..., 29.86%. The fibers are aligned in the x-direction and distributed in the RVE either uniformly (*aligned uniform* case) or "randomly" (*aligned "random" case*), with the restriction that each fiber can move only within its own "box" so that no contact of fibers will occur. Each fiber is discretized using 312 constant elements (Fig. 5), which have been found to be sufficient for obtaining converged BEM results. Each element or node has three degrees of freedom and each fiber has six unknown rigid-body motions.

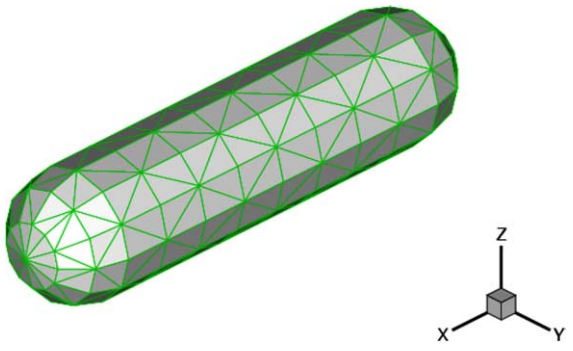

Fig. 5. A boundary element mesh used for the short fiber (length = 8, radius = 1, with 312 elements).

Thus, the largest BEM model in this example, with $10 \times 36 \times 36$ fibers, has a total degrees of freedom of 12,208,320 ($10 \times 36 \times 36 \times (312 \times 3 + 6)$).

Fig. 6 shows the RVE in the aligned "random" case with $10 \times 10 \times 10$ fibers and the contour stresses at the fiber–matrix interfaces. Again, the remote load (σ^{∞}) is applied in the x-direction only. High stress on the interface occurs when two fibers are closer to each other, indicating stronger interactions between the two fibers. Within each fiber, the high stress areas are at the two ends of the fiber. Fig. 7 gives the estimated effective longitudinal moduli of the composite models using Eq. (7), with the two data-collection surfaces being placed one-fiber inside the RVE in order to reduce the boundary effects. The BEM results are compared with the ones using Halpin–Tsai equation (Eq. (8)) and good agreement is observed, especially for lower fiber volume fractions. The results for the aligned "random" case is slightly lower than those for the aligned uniform case, although this difference vanishes at higher fiber volume fractions. Halpin–Tsai equation has been found to depart from the BEM results reported in Refs. [37,38] for higher fiber volume fractions and aspect ratios, which also occurs in Fig. 7. Revised Halpin–Tsai equations for such cases and more discussions on the applicability of the original Halpin–Tsai equation can be found in Refs. [37,38].

This short-fiber composite example demonstrates that the developed fast multipole BEM is correct and the RVE models employed are adequate (another verification of the developed BEM approach using analytical solutions for a rigid-sphere inclusion can be found in Ref. [42]).

4.3. Study of CNT composites

In this example, we study the effects of the CNT volume fractions on the effective moduli of the

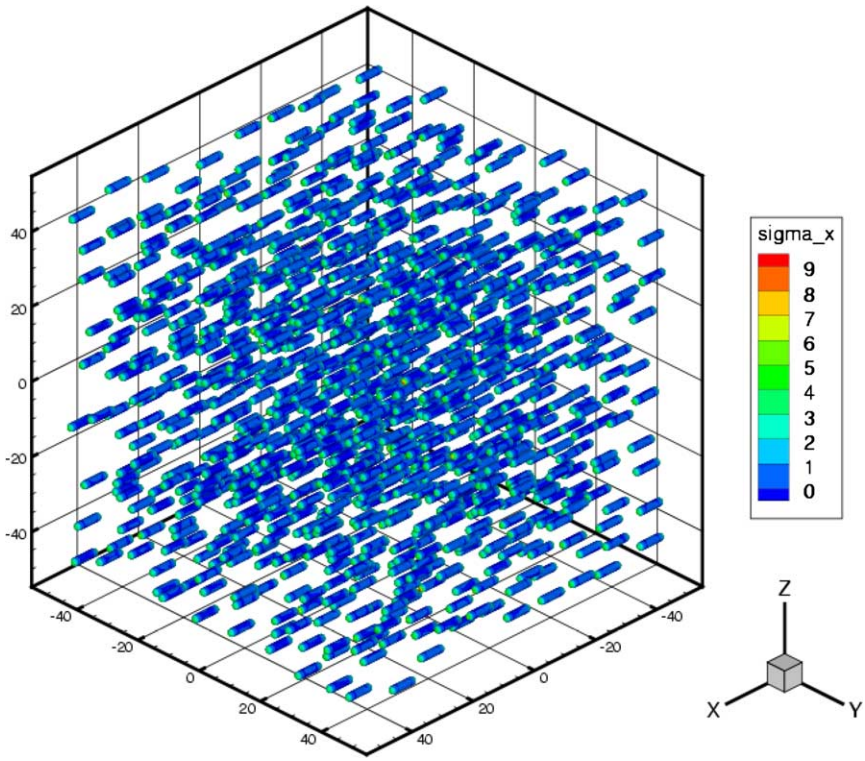

Fig. 6. Study of short-fiber composites with cubical RVEs containing $10 \times m \times m$ fibers: stress contour plot ($\times\sigma^{\infty}$) is shown for the RVE with $m = 10$ in the aligned "random" case (with fiber volume fraction = 2.30%).

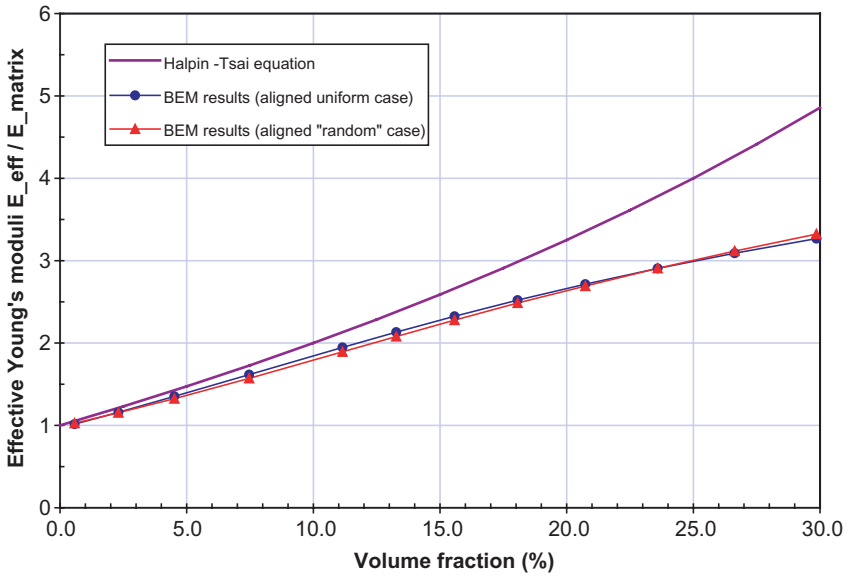

Fig. 7. Effective longitudinal moduli for the short-fiber composites predicted by the fast BEM.

CNT composites. The length of the CNT fibers is fixed at 50 nm, the radius of the CNT is 0.7 nm and the CNT thickness is 0.34 nm. The volume of the CNT is calculated by considering it as a hollow cylinder with the outer radius equal to 0.7 nm. For the matrix material, the NASA LaRC-SI polymer is used, with a Young's modulus of 3.8 GPa and Poisson's ratio of 0.4. All the above parameters are chosen from Ref. [18] for the comparison.

A boundary element mesh for the CNT fiber is shown in Fig. 8. Smaller elements are concentrated near the two ends of the tube since it has been shown that high stresses will occur near the tips of slender or line inclusions [29,42]. There are 600 triangular constant elements for one CNT in this mesh, which yields 1806 degrees of freedom per CNT fiber (600×3 plus 6 unknown rigid-body motions). This mesh was found to be sufficient for obtaining converged results for the estimated effective moduli. Two different distributions of the fibers in the RVE are considered, all arranged in arrays denoted by m_x, m_y and m_z being the number of CNTs in the x-, y-, and z-direction, respectively. The first case is a uniform distribution of aligned fibers, to be called the *aligned uniform* case. Arrays of $m_x \times m_y \times m_z$ CNT fibers are distributed evenly

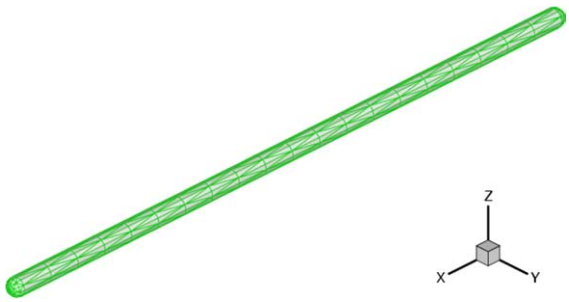

Fig. 8. A boundary element mesh used for the CNT (with 600 elements).

inside the RVE. However, positions of the CNTs in the x-direction are shifted, for every other CNT, a distance equal to half of the CNT length plus the gap between the CNTs in the x-direction. In this way, no weak regions (gaps) will exist in the RVE along the CNT direction. The second case is a "random" distribution of aligned CNT fibers, where the fibers are still aligned in the x-direction, but their locations are shifted randomly in the x-, y- and z-directions within certain ranges so that each fiber remains in its own "box" to avoid contact of the fibers. This case will be called the *aligned random* case. In both cases, the number

of CNTs in the x-direction, m_x is fixed, while the number of CNTs in the y- and z-directions, $m_y = m_z$ is increased in order to increase the volume fractions of the CNTs in the composites. The dimensions of the RVEs first studied in this case are $300 \times 60 \times 60$ nm^3, which are referred to as *small RVE* cases. Larger RVEs of the dimensions $600 \times 120 \times 120$ nm^3 are also studied, which will be referred to as *large RVE* cases.

Fig. 9 shows a contour plot of interface stress σ_x in the matrix for a small RVE containing 605 ($5 \times 11 \times 11$) aligned random CNT fibers, which can help to understand the load-transfer mechanism in the CNT composites. For each fiber, high stresses occur around the two ends of the fiber, which is consistent with the theory which predicts that in the limit as the slender inclusion becomes a rigid line, singularity of stresses exists at the two tips [29]. Values of these stresses are even higher when two CNTs are close to each other, suggesting closer interactions of the CNT fibers. The largest value of the stress is about 22 times of that of the applied stress σ^∞ in the far field. This stress plot is typical among all the studied RVEs, with CNTs being arranged in $5 \times m \times m$ arrays, with $m = 2, 4, 6, 8, 9, 10, 11, 12, 13, \ldots, 20$, in the small RVE cases. The small RVE with 2000 "random" CNTs is shown in Fig. 10. The large RVE models are obtained by simply repeating (once) the small RVE in the x-, y-, and z-direction, hence producing RVE models which are eight times the sizes of the corresponding small RVEs.

The estimated effective longitudinal Young's moduli (E_{eff}) of the CNT composites against the CNT volume fractions are plotted in Fig. 11, and compared with the data in Ref. [18] (Fig. 7 in Ref. [18], with CNT length = 50 nm). The BEM results were obtained for CNT volume fractions up to 10.48% due to the limitations on model sizes. All the results obtained by using the developed BEM approach based on the rigid-inclusion models are close to the results in Ref. [18] which are based on the MD and a multiscale approach. For the small RVE cases, the results for the aligned random and uniform cases are very close, possibly due to the fact that the random cases

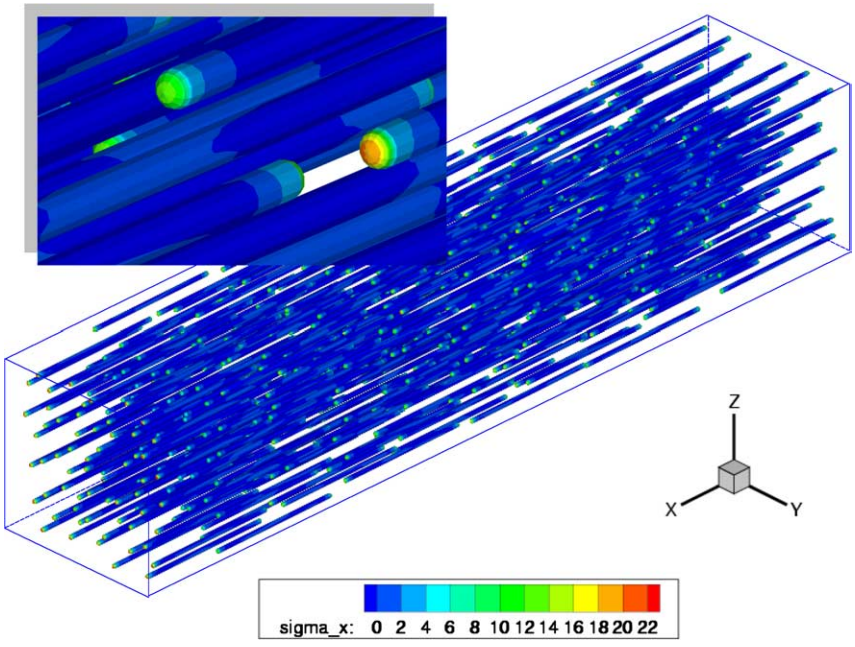

Fig. 9. Load transfer in the CNT composite model: contour plot of surface stresses ($\times\sigma^\infty$) for a small RVE with 605 "randomly" distributed and aligned CNT fibers (with length = 50 nm, volume fraction = 3.17%. The insert shows the high stress areas when two fibers come closer.).

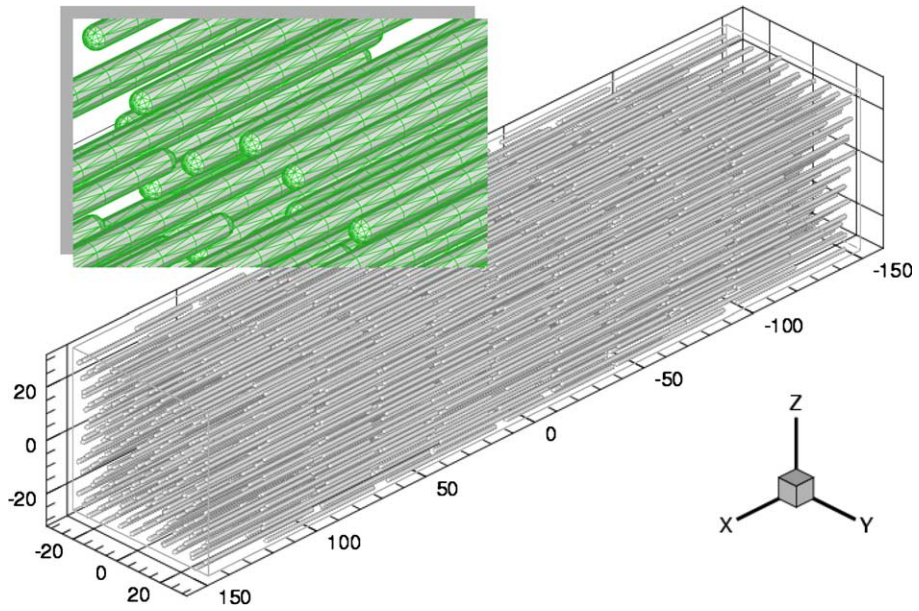

Fig. 10. A small RVE containing 2000 CNT fibers with the total DOF = 3,612,000 (with CNT length = 50 nm, volume fraction = 10.48%. The insert shows a close-up of the tubes with the boundary element mesh.).

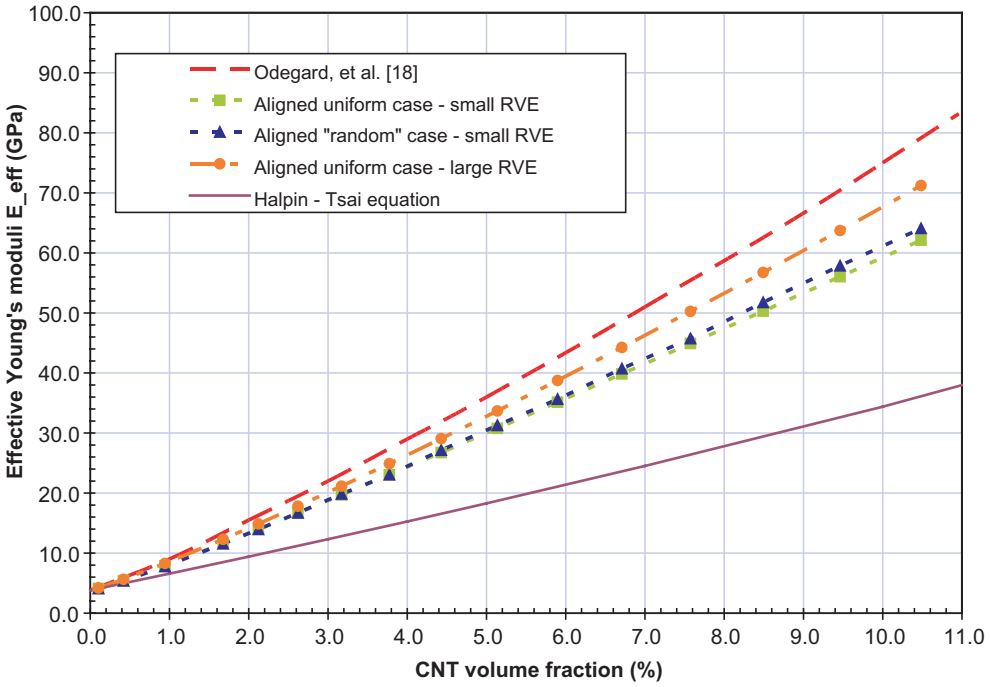

Fig. 11. Estimated effective longitudinal moduli of the CNT composite models in the CNT direction as a function of the CNT volume fraction (CNT length = 50 nm).

are only slight perturbations of the corresponding uniform ones. The results in the large RVE show significant improvement (half way closer to the curve from Ref. [18]). The curve by Halpin–Tsai equation is also shown in the figure for reference. The departure of Halpin–Tsai curve with the others may be due to the larger aspect ratios of the CNT fibers in this case (see, e.g., discussions in Refs. [37,38]). Because of the lack of means to generate RVE models with randomly distributed and randomly oriented fibers without causing contact of the fibers, such RVEs were not attempted. Better RVEs can be made in the future to account for more realistic arrangements of the CNT fibers in a composite.

All the jobs for the examples were run on a FUJITSU PRIMEPOWER HPC2500 computer, which is a shared memory machine having 128 CPUs with 1.5 GHz speed and 512 GB memory, and located at the Kyoto University. The simulation jobs used 32 CPUs. No serious attempts were made to parallelize the code except for the use of a few OpenMP directives and automatic parallelization made by the compiler. The largest RVE with 16,000 CNT fibers (eight times larger than the small RVE shown in Fig. 10) has a total DOF of 28,896,000 ($16{,}000 \times (600 \times 3 + 6)$). The developed multipole BEM code run smoothly and delivered the solution of the BIE equations within 34 h (wall-clock time) for this very large BEM model.

5. Discussions

The BEM results based on the rigid-fiber model are shown to be very close with the reported data in Ref. [18] which is based on MD combined with an equivalent-continuum model. Although surprising, it is also expected based on the results in Refs. [20,21] that already show strong correlation of the MD-based multiscale results and the continuum mechanics results. Furthermore, the MD model for obtaining the properties of the effective fibers in Ref. [18] assumes a strong bond (using PmPV molecules) between the CNT and polymer, which may be close to the perfect bonding assumptions used in the current rigid-fiber model.

From the results in this paper and others reported in Refs. [18,20,21], it seems that the micromechanics models of the CNT composites are adequate for the evaluations of their *overall* mechanical properties, such as the effective moduli of such composites. Especially in the case of long, straight CNT fibers, even the traditional rule of mixtures may be sufficient to be applied as a first approximation, as have been used in various studies of the CNT composites [14,15,20,21]. The MD approach and MD-based multiscale approaches can be employed in studies focused on the interface properties and potential failure modes of the CNT-reinforced composites.

The new fast multipole BEM based on the rigid-inclusion model for the analysis of CNT composites can find many applications in the studies of CNT composites where large models are deemed necessary. For example, interactions of the CNT fibers, load transfer mechanisms and effective properties of a composite can be investigated readily using the BEM with different parameters, such as CNT aspect ratios, volume fractions, distributions and orientations in the matrix. However, the rigid-inclusion model has some obvious limitations. For example, the effect of the ratio of the Young's modulus of the CNT to that of the matrix for a composite can not be accounted for in this rigid-inclusion model, which is assumed to be infinity in the rigid-inclusion model for any matrix material. Another important issue is the effect of the temperature on the mechanical behaviors of the CNT composites, which has not been considered in the developed BEM models. At different temperatures, especially high temperatures, the CNT composites will behave differently, such as nonlinearly with plastic deformations. Presumably the interface regions may behave differently as well. How to address the temperature effect in a continuum or multiscale model will be a challenging task that needs to be studied in the future.

The developed BEM can be extended readily to account for more complicated physics or interactions of the CNTs in a matrix. Elasticity of the CNTs can be introduced in this model to replace the assumption of rigidity. An effective-fiber model based on the MD similar to the one developed in Ref. [18] can also be combined with the fast

multipole BEM models. With the development in computing hardware, it is quite possible in the near future to directly combine the MD model for the CNTs and the BEM model for the matrix to have a multiscale method that can handle larger models and account for more intricate physics in CNT-reinforced composites, such as more realistic interface properties, debonding or other failure modes, besides evaluations of their effective properties.

6. Conclusion

A new fast multipole boundary element method is applied in the modeling of CNT-reinforced composites in this paper. The CNTs are treated as rigid fibers in this approach due to their exceptionally high stiffness compared with commonly used polymer matrix materials. Justifications of this seemingly naïve approach is provided and verified with some preliminary results using the developed BEM. The estimated effective Young's moduli using this rigid-fiber model and the BEM are found to be very close to those obtained using an MD-based multiscale approach reported in the literature. The largest model studied contains 16,000 CNT fibers and has the total degrees of freedom above 28.8 millions. These results clearly demonstrate the effectiveness, efficiency and promises of the developed fast multipole BEM as a fast and first-order numerical tool for large-scale characterizations of the carbon-nanotube composites. Elasticity of the CNT fibers and more realistic interface conditions based on MD simulation results of CNT composites can be incorporated readily in this fast multipole BEM.

Acknowledgments

The first author (Y.J.L.) would like to acknowledge the support of the Japan Society for the Promotion of Science (JSPS) fellowship and the Academic Center for Computing and Media Studies of the Kyoto University. The authors thank Dr. D. Qian and Mr. V. Mokashi at the University of Cincinnati for sharing the MD simulation result shown in Fig. 1.

References

[1] E.T. Thostenson, Z.F. Ren, T.-W. Chou, Advances in the science and technology of carbon nanotubes and their composites: a review, Compos. Sci. Technol. 61 (2001) 1899–1912.
[2] R.S. Ruoff, D.C. Lorents, Mechanical and thermal properties of carbon nanotubes, Carbon 33 (7) (1995) 925–930.
[3] J.P. Lu, Elastic properties of single and multilayered nanotubes, J. Phys. Chem. Solids 58 (11) (1997) 1649–1652.
[4] Z.F. Ren, Z.P. Huang, J.W. Xu, J.H. Wang, P. Bush, M.P. Siegal, P.N. Provencio, Synthesis of large arrays of well-aligned carbon nanotubes on glass, Science 282 (5391) (1998) 1105–1107.
[5] D. Qian, E.C. Dickey, R. Andrews, T. Rantell, Load transfer and deformation mechanisms in carbon nanotube–polystyrene composites, Appl. Phys. Lett. 76 (20) (2000) 2868–2870.
[6] E.W. Wong, P.E. Sheehan, C.M. Lieber, Nanobeam mechanics: elasticity, strength, and toughness of nanorods and nanotubes, Science 277 (5334) (1997) 1971–1975.
[7] K. Sohlberg, B.G. Sumpter, R.E. Tuzun, D.W. Noid, Continuum methods of mechanics as a simplified approach to structural engineering of nanostructures, Nanotechnology 9 (1) (1998) 30–36.
[8] S. Govindjee, J.L. Sackman, On the use of continuum mechanics to estimate the properties of nanotubes, Solid State Commun. 110 (4) (1999) 227–230.
[9] C.Q. Ru, Column buckling of multiwalled carbon nanotubes with interlayer radial displacements, Phys. Rev. B 62 (24) (2000) 16962–16967.
[10] C.Q. Ru, Axially compressed buckling of a doublewalled carbon nanotube embedded in an elastic medium, J. Mech. Phys. Solids 49 (6) (2001) 1265–1279.
[11] D. Qian, W.K. Liu, R.S. Ruoff, Mechanics of C_{60} in nanotubes, J. Phys. Chem. B 105 (44) (2001) 10753–10758.
[12] R.B. Pipes, P. Hubert, Helical carbon nanotube arrays: mechanical properties, Compos. Sci. Technol. 62 (3) (2002) 419–428.
[13] Y.J. Liu, X.L. Chen, Continuum models of carbon nanotube-based composites using the boundary element method, Electron. J. Bound. Elements 1 (2) (2003) 316–335.
[14] Y.J. Liu, X.L. Chen, Evaluations of the effective materials properties of carbon nanotube-based composites using a nanoscale representative volume element, Mech. Mater. 35 (1-2) (2003) 69–81.
[15] X.L. Chen, Y.J. Liu, Square representative volume elements for evaluating the effective material properties of carbon nanotube-based composites, Comput. Mater. Sci. 29 (1) (2004) 1–11.
[16] F.T. Fisher, R.D. Bradshaw, L.C. Brinson, Effects of nanotube waviness on the modulus of nanotube-reinforced polymers, Appl. Phys. Lett. 80 (24) (2002) 4647–4649.
[17] F.T. Fisher, R.D. Bradshaw, L.C. Brinson, Fiber waviness in nanotube-reinforced polymer composites—I: Modulus

predictions using effective nanotube properties, Compos. Sci. Technol. 63 (11) (2003) 1689–1703.
[18] G.M. Odegard, T.S. Gates, K.E. Wise, C. Park, E.J. Siochi, Constitutive modeling of nanotube-reinforced polymer composites, Compos. Sci. Technol. 63 (11) (2003) 1671–1687.
[19] G.M. Odegard, T.S. Gates, L.M. Nicholson, K.E. Wise, Equivalent-continuum modeling of nano-structured materials, Compos. Sci. Technol. 62 (14) (2002) 1869–1880.
[20] G.M. Odegard, R.B. Pipes, P. Hubert, Comparison of two models of SWCN polymer composites, Compos. Sci. Technol. 64 (7-8) (2004) 1011–1020.
[21] M. Griebel, J. Hamaekers, Molecular dynamics simulations of the elastic moduli of polymer–carbon nanotube composites, Comput. Methods Appl. Mech. Engrg. 193 (2004) 1773–1788.
[22] M.M.J. Treacy, T.W. Ebbesen, J.M. Gibson, Exceptionally high Young's modulus observed for individual carbon nanotubes, Nature 381 (6584) (1996) 678–680.
[23] J.P. Lu, Elastic properties of carbon nanotubes and nanopores, Phys. Rev. Lett. 79 (7) (1997) 1297–1300.
[24] M. Buongiorno Nardelli, J.-L. Fattebert, D. Orlikowski, C. Roland, Q. Zhao, J. Bernholc, Mechanical properties, defects and electronic behavior of carbon nanotubes, Carbon 38 (11-12) (2000) 1703–1711.
[25] C. Li, T.-W. Chou, Elastic moduli of multi-walled carbon nanotubes and the effect of van der Waals forces, Compos. Sci. Technol. 63 (11) (2003) 1517–1524.
[26] V. Mokashi, D. Qian, Y.J. Liu, Interfacial mechanics in nanocomposites reinforced by single-walled carbon nanotubes, in preparation.
[27] J. Gou, B. Minaie, B. Wang, Z.Y. Liang, C. Zhang, Computational and experimental study of interfacial bonding of single-walled nanotube reinforced composites, Comput. Mater. Sci. 31 (3–4) (2004) 225–236.
[28] T. Mura, Micromechanics of Defects in Solids, second, revised ed., Kluwer Academic Publishers, Dordrecht, 1987.
[29] J. Dundurs, X. Markenscoff, A Green's function formulation of anticracks and their interaction with load-induced singularities, J. Appl. Mech. 56 (3) (1989) 550–555.
[30] K.X. Hu, A. Chandra, Interactions among general systems of cracks and anticracks—an integral-equation approach, J. Appl. Mech. 60 (4) (1993) 920–928.
[31] K.X. Hu, Y. Huang, A microcracked solid reinforced by rigid-line fibers, Compos. Sci. Technol. 49 (2) (1993) 145–151.
[32] K.X. Hu, A. Chandra, Y. Huang, On crack, rigid-line fiber, and interface interactions, Mech. Mater. 19 (1) (1994) 15–28.
[33] A. Chandra, Y. Huang, X. Wei, K.X. Hu, A hybrid micro–macro BEM formulation for micro-crack clusters in elastic components, Int. J. Numer. Methods Engrg. 38 (7) (1995) 1215–1236.
[34] Y. Huang, K.X. Hu, A. Chandra, Stiffness evaluation for solids containing dilute distributions of inclusions and microcracks, J. Appl. Mech. 62 (1) (1995) 71–77.
[35] L.G.S. Leite, H.B. Coda, W.S. Venturini, Two-dimensional solids reinforced by thin bars using the boundary element method, Engrg. Anal. Bound. Elements 27 (2003) 193–201.
[36] C.Y. Dong, S.H. Lo, Y.K. Cheung, Interaction between cracks and rigid-line inclusions by an integral equation approach, Comput. Mech. 31 (2003) 238–252.
[37] T.D. Papathanasiou, M.S. Ingber, D.C. Guell, Stiffness enhancement in aligned, short-fibre composites: a computational and experimental investigation, Compos. Sci. Technol. 54 (1) (1995) 1–9.
[38] M.S. Ingber, T.D. Papathanasiou, A parallel-supercomputing investigation of the stiffness of aligned, short-fiber-reinforced composites using the boundary element method, Int. J. Numer. Methods Engrg. 40 (1997) 3477–3491.
[39] S. Mukherjee, Boundary Element Methods in Creep and Fracture, Applied Science Publishers, New York, 1982.
[40] P.K. Banerjee, The Boundary Element Methods in Engineering, second ed., McGraw-Hill, New York, 1994.
[41] C.A. Brebbia, J. Dominguez, Boundary Elements—An Introductory Course, McGraw-Hill, New York, 1989.
[42] Y.J. Liu, N. Nishimura, Y. Otani, T. Takahashi, X.L. Chen, H. Munakata, A fast boundary element method for the analysis of fiber-reinforced composites based on a rigid-inclusion model, J. Appl. Mech. 72 (1) (2005) 115–120.
[43] N. Nishimura, Fast multipole accelerated boundary integral equation methods, Appl. Mech. Rev. 55 (4) (2002) 299–324.
[44] L.F. Greengard, J. Helsing, On the numerical evaluation of elastostatic fields in locally isotropic two-dimensional composites, J. Mech. Phys. Solids 46 (8) (1998) 1441–1462.
[45] L.F. Greengard, M.C. Kropinski, A. Mayo, Integral equation methods for Stokes flow and isotropic elasticity in the plane, J. Comput. Phys. 125 (1996) 403–414.
[46] J. Helsing, An integral equation method for elastostatics of periodic composites, J. Mech. Phys. Solids 43 (6) (1995) 815–828.
[47] L.F. Greengard, V. Rokhlin, A fast algorithm for particle simulations, J. Comput. Phys. 73 (2) (1987) 325–348.
[48] Y. Fu, K.J. Klimkowski, G.J. Rodin, E. Berger, J.C. Browne, J.K. Singer, R.A.V.D. Geijn, K.S. Vemaganti, A fast solution method for three-dimensional many-particle problems of linear elasticity, Int. J. Numer. Methods Engrg. 42 (1998) 1215–1229.
[49] T. Takahashi, S. Kobayashi, N. Nishimura, Fast multipole BEM simulation of overcoring in an improved conical-end borehole strain measurement method, in: Z.H. Yao (Ed.), Mechanics and Engineering—In Honor of Professor Qinghua Du's 80th Anniversary, Tsinghua University Press, Beijing, 1999, pp. 120–127.
[50] K. Yoshida, Applications of fast multipole method to boundary integral equation method, Ph.D. dissertation, Department of Global Environment Engineering, Kyoto University, 2001.